Research Paper
J. Astron. Space Sci. 42(2), 39-46 (2025)
https://doi.org/10.5140/JASS.2025.42.2.39

JASS Journal of Astronomy and Space Sciences

Classification of Ionograms Obtained from Vertical Incidence Pulsed Ionospheric Radar (VIPIR)/Dynasonde Ionospheric Radar at Jang Bogo Station, Antarctica

Junho Back[1,2], Geonhwa Jee[2,3], Hyuck-Jin Kwon[2†], Khan-Hyuk Kim[1], Changsup Lee[2,3], Young-Bae Ham[2,3], Nikolay Zabotin[4]

[1]School of Space Research, Kyung Hee University, Yongin 17104, Korea
[2]Korea Polar Research Institute, Incheon 21990, Korea
[3]University of Science and Technology, Daejeon 34113, Korea
[4]Cooperative Institute for Research in Environmental Sciences, University of Colorado, Boulder, CO 80309, USA

The electron density profiles produced from the ionospheric sounding system are traditionally estimated by the inversion procedure based on the image analysis of the observed ionograms. Jang Bogo Vertical Incidence Pulsed Ionospheric Radar (VIPIR) with Dynasonde (hereafter, JVD), however, uses the three-dimensional electron density inversion approach named "NeXtYZ" to produce ionospheric density, ion velocity, and tilt of the ionization in the bottomside ionosphere based on the list of detected radio echoes with their physical parameters. Sometimes, the resulting density profiles can be erroneous, not reflecting real ionosphere, probably due to severely disturbed ionosphere in the polar region. In this study, the automatic classification procedure of the estimated electron density profiles is developed to filter out unusable data for the 5-year period from 2017 to 2021. The ionograms are classified into four categories: 'Unavailable', 'Sporadic E', 'Needs Reprocessing', and 'Available'. It is found that approximately 50% of ionograms are evaluated to be reasonable with proper electron density profiles and about 35% of them tend to be affected by sporadic-E like structures, blocking the F-region ionosphere to be observed. It should be noted that the sporadic-E like structures in the polar ionosphere seems to be main obstacles for the ionospheric sounding observation of the F-region ionosphere. Only less than 10% of ionograms are classified as a reprocessing type which needs to be reprocessed. Finally, no echoes are recognized by Dynasonde analysis for about 5% of ionograms. The reprocessing and/or unavailable types might be associated with auroral precipitations that disturbs the ionosphere in the polar region.

Keywords: ionogram, Vertical Incidence Pulsed Ionospheric Radar (VIPIR), Dynasonde, polar ionosphere

1. INTRODUCTION

The ionosphere in the polar region has a critical importance for the global upper atmosphere from the space weather perspective since the major part of solar energy affecting the upper atmosphere is absorbed through the polar ionosphere due to the characteristics of the Earth's magnetic field (Heelis 1982; Carlson 1994; Fontaine 2002). In order to monitor the polar ionosphere, many of the incoherent scatter radar (ISR), the most versatile ground-based instrument for the ionosphere, are located in the northern polar region. These are, for example, European Incoherent Scatter Scientific Association (EISCAT) in Scandinavia and Svalbard, Sondrestrom ISR in Greenland, Poker Flat ISR (PFISR) in Alaska, Resolute Bay ISRs (RISR-N and RISR-C) in Resolute Bay, Canada. However, the ISR facilities are extremely expensive not only to build them but also to maintain, and therefore they are not usually available for routine observations of the ionosphere but rather utilized for campaign-based observations. Another common observation technique for the ionosphere is the ionospheric

This is an Open Access article distributed under the terms of the Creative Commons Attribution Non-Commercial License (https://creativecommons.org/licenses/by-nc/3.0/) which permits unrestricted non-commercial use, distribution, and reproduction in any medium, provided the original work is properly cited.

Received 05 APR 2025 **Revised** 09 MAY 2025 **Accepted** 21 MAY 2025
†**Corresponding Author**
Tel: +82-32-760-5375, E-mail: hjkwon@kopri.re.kr
ORCID: https://orcid.org/0000-0001-9670-0711

sounders which are relatively affordable instruments for both installation and maintenance but provide data only for the bottom-side ionosphere while the ISR can observe the entire ionosphere (Scali et al. 1997; Ham et al. 2020). The ground-based ionospheric sounding systems such as Digisondes and Dynasondes are globally distributed to routinely monitor the state of the ionosphere (i.e., the global ionospheric radio observatory (GIRO) digisonde network: https://giro.uml.edu/index.html or the Dynasonde Database http://surf.colorado.edu). However, the global distribution of ionospheric sounding systems is highly asymmetric, with most of them located in the northern hemisphere and sparse locations in the southern hemisphere. In fact, the southern polar region is extremely limited to install and maintain ground-based observational facilities and therefore there are only a few ionospheric radars in the region. The hemispheric asymmetry of the ground-based observations is one of the major problems in understanding the global upper atmosphere including the ionosphere.

The Korea Polar Research Institute (KOPRI) established the Jang Bogo Station (JBS), the second Korean Antarctic station in 2014 at Terra Nova Bay in Northern Victoria Land, Antarctica [74.62°S, 164.22°E in geographic; 79.87°S, 53.56°W in Altitude Adjusted Corrected Geomagnetic (AACGM) (Shepherd 2014)]. In this ideal location for observing the characteristics of the polar cap boundary, KOPRI has been operating various optical and radar instruments, including Fabry-Perot interferometer (FPI), all-sky auroral and airglow imagers, GNSS scintillation monitor, magnetometers, neutron monitor, and ionospheric radar (Kwon et al. 2018; Ham et al. 2020; Jee et al. 2021; Kwon et al. 2022; Kim et al. 2023). The ionospheric radar, Jang Bogo Vertical Incidence Pulsed Ionospheric Radar (VIPIR) with Dynasonde (JVD) analysis routinely monitors the states of the bottom-side ionosphere, producing vertical profiles of ionospheric parameters such as electron density, ionospheric tilts (i.e., horizontal gradient of the ionospheric density), and ion velocity from the inversion scheme called the NeXtYZ within the Dynasonde analysis (Zabotin et al. 2006).

Since the JVD is the only Dynasonde instrument operated in the southern polar region, the observed ionospheric parameters need to be evaluated in comparison with other independent measurements. For instance, Kim et al. (2022) compared the JVD ionospheric density with GPS total electron content (TEC) simultaneously measured at JBS during the solar minimum period of 2017–2019. They found that the electron density at F2-layer and bottomside TEC from the JVD show a good correlation with GPS TEC under quiet condition but less so during disturbed periods. The validation of JVD ion velocity measurement was also done by comparing SuperDARN observations simultaneously performed over JBS (Kwon et al. 2024). The comparison between ion drift velocity obtained from JVD and line-of-sight Doppler velocity measured by SuperDARN shows generally a good agreement and the correlation coefficient between them increases as geomagnetic activity increases, which is associated with characteristics of the two measurements (Kwon et al. 2024).

On the other hand, the ionospheric profile products from the Dynasonde analysis haven't been evaluated since the JVD started its operation in 2017. The severely disturbed ionosphere in the polar region, particularly during storm periods, may produce irregular ionograms in the ionospheric sounding observations like the JVD, which may be challenging for the Dynasonde analysis. In fact, it is occasionally found that the JVD does not produce proper ionospheric density profiles during auroral occurrences, as will be presented later in this study. Therefore, it is necessary to evaluate the accuracy of the analysis procedure within the Dynasonde by directly comparing estimated ionospheric parameters with ionogram images obtained from the radar.

In the following sections, the inversion scheme of the Dynasonde is briefly reviewed before describing classification procedure in Section 3. In Section 4, the results and discussions are presented and then summarized and concluded in the last section.

2. NeXtYZ INVERSION PROCEDURE

The NeXtYZ 3-D inversion procedure is adopted for the JVD observations to produce three-dimensional distribution of electron density over the JBS, including the vertical profiles of electron density with horizontal gradients and ion velocity (Zabotin et al. 2006; Ham et al. 2020). The NeXtYZ uses a numerical multiple ray-tracing method to calculate the 3D electron density distribution by analyzing the group delay and angles of arrival for the ionospheric echoes for each ionogram. This procedure is performed by dividing the ionosphere into thin plasma frequency layers, shaped as wedges, and solves a least squares optimization problem that minimize the residuals between measured and calculated propagation times and directions of all echoes. The inversion procedure begins from the bottom of the profile in a series of plasma frequency layers. Near the F-region peak, the optimization problem is solved for the Chapman model, instead of another plasma wedge at the height (Zabotin et al. 2006).

Fig. 1 shows a typical ionogram image obtained from JVD. The upper panel represents the ranges of ionospheric

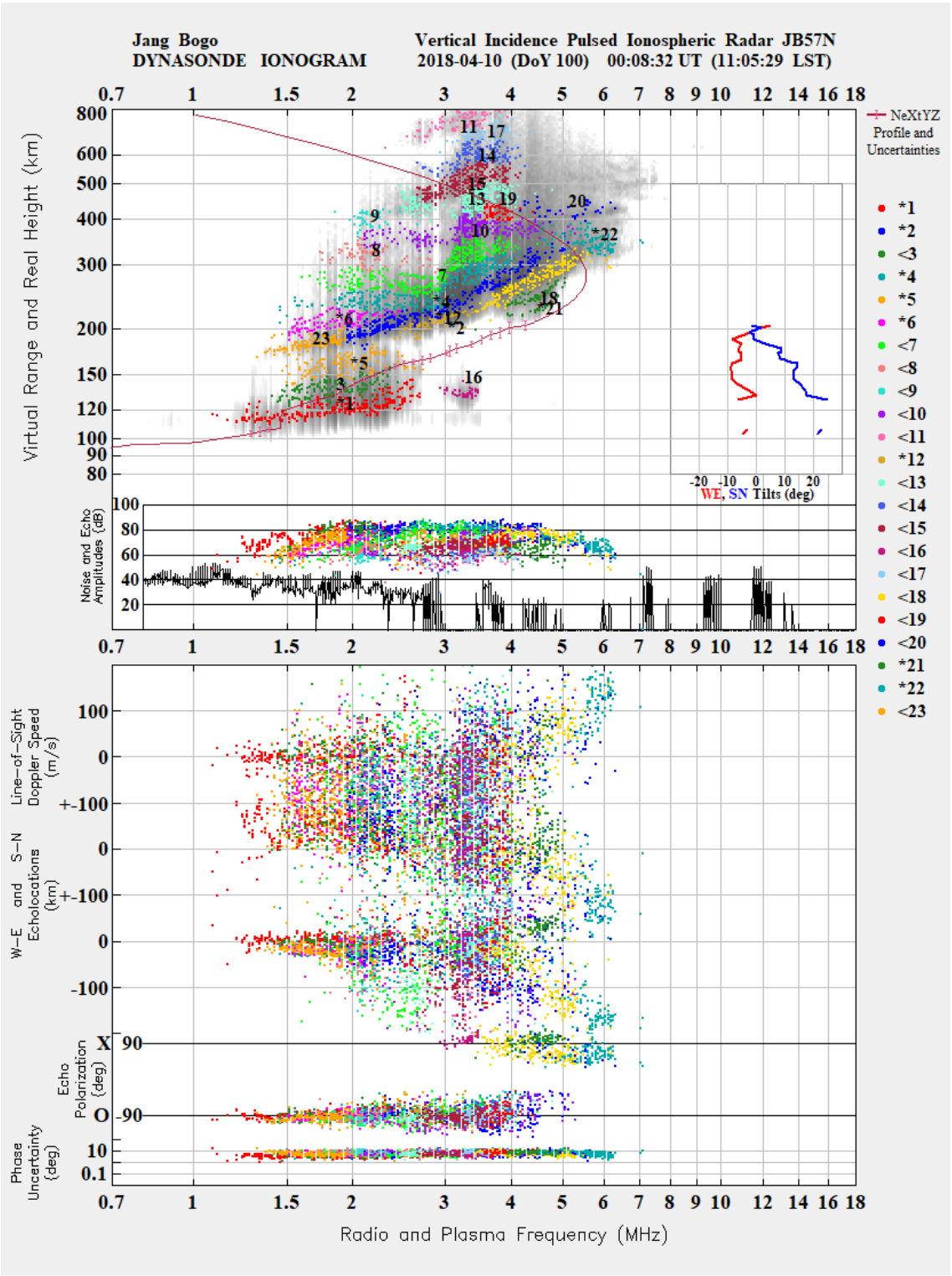


Fig. 1. Sample ionogram with specific information of the echoes and ionospheric products including electron density profile, ion velocity, and tilts of the ionization layers produced by VIPIR/Dynasonde at JBS (JVD). The x-axis and y-axis of the top panel represent plasma/radio frequency and virtual/real height of the ionosphere, respectively. The gray images in the top panel represent the Signal-to-Noise Ratio, and radio echoes are displayed as colored dots. The numbered groups of different colored dots indicate traces. The red and blue lines in the insert of the top panel show profiles of the tilt angles of the local reflecting ionospheric surfaces in the east-west and north-south directions, respectively. VIPIR, Vertical Incidence Pulsed Ionospheric Radar; JBS, Jang Bogo Station; JVD, Jang Bogo Vertical Incidence Pulsed Ionospheric Radar with Dynasonde analysis.

echoes and the electron density profile with error bars in the bottom-side profile and shows the amplitude of echoes (color) and noise (black) in decibel at the bottom of the panel. The additional information about the echoes, line-of-sight Doppler speed, horizontal echo locations, polarization and phase uncertainty, are shown in the bottom panel. The x-axis and y-axis in the upper panel indicate radio and plasma frequencies and virtual and real height of the ionosphere, respectively. The gray background image in the Fig. 1 is the traditional amplitudes-based (or Signal-to-Noise Ratio, SNR-based) ionogram representation. The colored dots indicate the recognized echoes to be used by the Dynasonde analysis for the estimation of ionospheric parameters (Wright & Pitteway 1999). SNR image and echoes are presented in the virtual height coordinate on the y-axis of the top panel. Each group of echoes with similar physical parameters (e.g., travel time, phase, polarization, direction of arrival, amplitude, and reflection altitude) forms classes of echoes or a "traces" marked with different colors and numbers. Note that only a few traces with asterisked numbers are selected for the inversion procedure. Each selected trace contains at least 10 echoes to ensure reasonable computational load. The trace includes both O-mode and X-mode polarization types, and passes an optimization procedure alternately minimizing the group range residuals and the ground return distance. Echoes are excluded from the process if their calculated reflection points lie outside the current wedge. This selection enables a more stable and accurate estimation of ionospheric parameters. The resulting electron density profile of the bottomside ionosphere is presented by the purple line with error bars in the real height coordinate. The error bars in the bottom-side electron density profile indicate error estimates (determined by NeXtYZ) for the real height. The part of the density profile for the topside ionosphere without error bars is estimated as a data-driven fit of the Chapman physics-based model (Zabotin et al. 2006). The red line and the blue line in the right box in the insert box of the upper panel indicate the local tilt angles of in the zonal and meridional directions, which is one of the unique results of the Dynasonde analysis because it assumes the wedge-stratified ionosphere (WSI), instead of simple plane-stratified ionosphere used by other conventional ionosonde observations.

The autonomous Dynasonde analysis is very robust in the echo detection. Most noticeable blunders are made at the upper-level processing stage, during the trace selection for further inversion procedures. And sometimes the critical frequency calculations are failing. These are two points in the analysis where interference of a skilled operator would allow to correct almost all errors of the autonomous analysis. Since the echo information is kept in the database, together with all necessary parameters of the sounding mode and of the original analysis, a reprocessing originated by an operator can be performed without invoking the raw data file. A very compact and intuitive web interface for the Expert Reprocessing function is available at the local Dynasonde installation.

3. CLASSIFICATION

As mentioned earlier, the Dynasonde analysis procedure sometimes fails to produce proper density profiles, in particular, during disturbed periods in the polar region and therefore, it may be necessary to evaluate the performance of the analysis procedure by directly comparing the produced density profiles with corresponding ionograms. For this purpose, we attempt to classify the Dynasonde outputs into four categories. Fig. 2 presents a simplified flowchart of the classification procedure used in the study. Automatically generated ionograms within the Dynasonde are classified into four categories by using sequential classification filters, as presented in Fig. 3: Four types of ionograms are denoted as Unavailable (a), Sporadic E (b), Needs Reprocessing (c), and Available (d). Figs. 3(a)–3(d) show the examples of the four types of ionograms. The ionograms as shown in Fig. 3(a) are classified as 'Unavailable' when no echoes (colored dots in the ionograms) are determined by the Dynasonde. Then, the filter picks out the ionograms with the signature of strong sporadic E layer capable of blanketing, as shown in Fig. 3(b), that can block radio signals from reaching the F-region ionosphere, which is classified as 'Sporadic E'. Next, the trace selection and profile inversion procedures are evaluated by comparing the produced density profiles with corresponding group of echo traces in the ionograms. If the density profiles do not look reasonable comparing with corresponding echo traces as the case of Fig. 3(c), they are classified as 'Needs Reprocessing' which may require to go through the inversion procedure again. To determine whether the echo trace is reasonable, the classification code compare the number of pixels occupied by the gray SNR image and the colored echo and utilizes the profile's gradient to verify whether the profile sharply drops at a certain altitude. Finally, all the remaining ionograms as shown in Fig. 3(d) are classified 'Available', which means that these can be utilized for the study on the ionosphere over the JBS without alteration. The four types of the ionograms are summarized in Table 1.

The 'Available' type provides sufficiently reliable electron

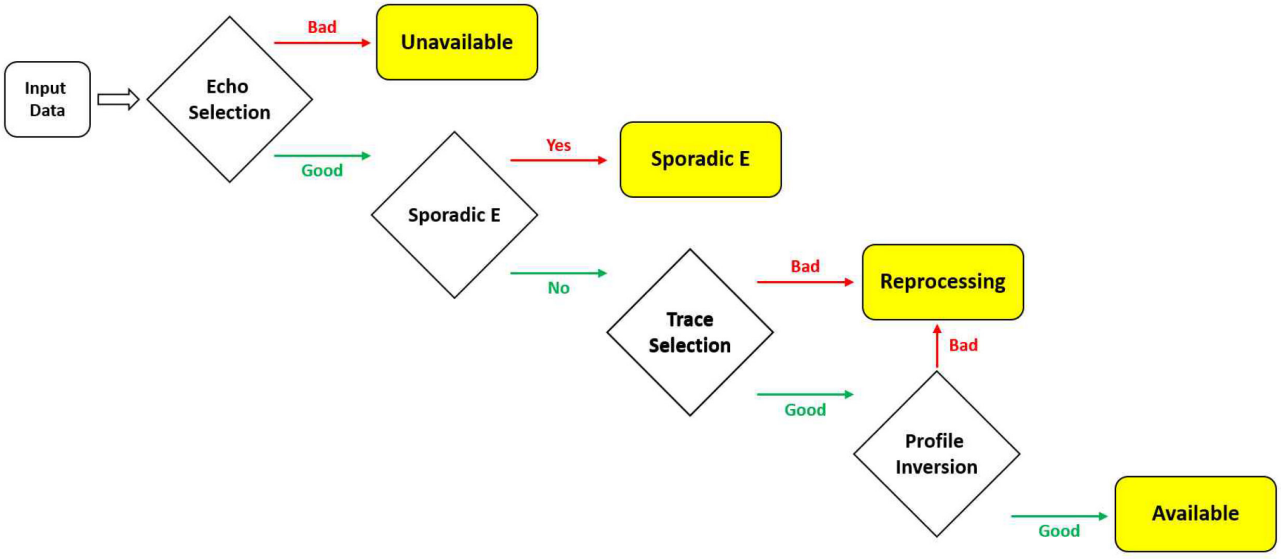


Fig. 2. Flowchart of the ionogram classification procedure.

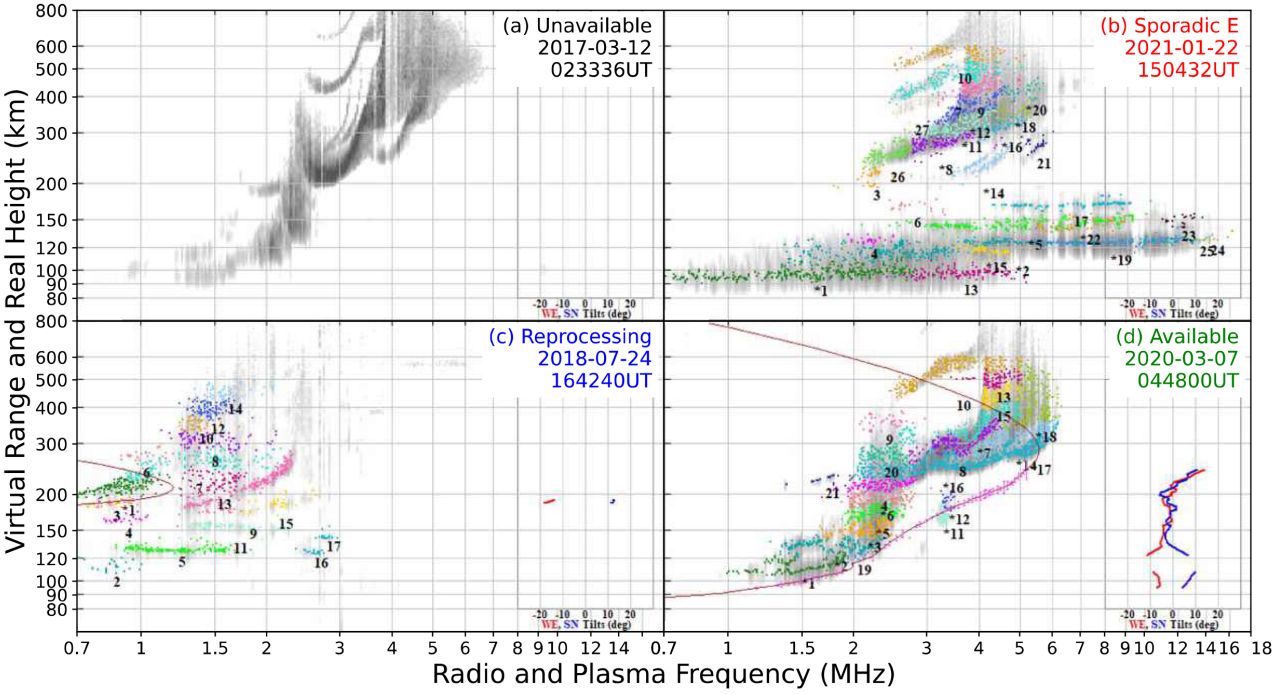


Fig. 3. Examples of the ionograms of four types as denoted.

density profiles derived from radio echoes, making it suitable for statistical studies of the ionospheric F layer, except for ionograms that contain sporadic-E like structures or present unreasonable profiles that poorly represents the echoes. This dataset inherently includes ionospheric events such as spread F, extremely low plasma densities, and auroral activity, as these phenomena are reflected in the electron density profiles through extremely high or low values of key parameters, such as the F layer maximum plasma frequency (FMXF) and its corresponding altitude (HMXF). For example, frequency spread F (FSF) represent abnormally high FMXF value. The echo of FSF spread along frequency in the ionospheric F layer, which is caused by scattering from ionospheric irregularities (Kintner et al. 2007). In contrast,

Table 1. Dynasonde ionograms are classified into four categories

Tpye	Description
Unavailable	No echoes are detected by the Dynasonde analysis.
Sporadic E	F-region ionosphere was blanketed by the sporadic-E like structure at lower altitudes.
Needs Reprocessing	Trace selection procedure was not properly performed in the autonomous Dynasonde analysis.
Available	Electron density profiles are properly produced.

range spread F (RSF) provides anomalously high HMXF values. In that case, echo is spreading along the height axis because of reflection from the multiple layers caused by the irregular ionospheric structure. (Afolayan et al. 2019; Wang et al. 2019). Consequently, ionospheric disturbances that cause spread F can lead to variation in parameters such as FMXF or HMXF in ionograms. However, to accurately identify spread F, additional information such as the GNSS scintillation index is required. In this study, events were classified based on the characteristics of ionograms therefore, spread F events were not explicitly categorized.

The classification procedure described above was performed by the Python-based automated classification code with Python Imaging Library (PIL) which provides RGB values of each pixel of the ionogram images, as if it was conducted by the human eye. To classify sporadic E, for example, following the URSI handbook of ionogram interpretation and reduction (Piggott & Rawer 1978), the height range of the ionospheric E layer was set approximately from 95 km to 150 km based on not only the vertical gradients of plasma density but also the presence of high-density plasma echoes.

4. RESULTS AND DISCUSSIONS

We conducted a random sampling to verify the reliability of the classification code used for this study. The sampling size was calculated by the Krejcie & Morgan formula (Krejcie & Morgan 1970):

$$n \geq \frac{\chi^2 \times \mathrm{N} \times \mathrm{p} \times (1-\mathrm{p})}{\mathrm{e}^2 \times (\mathrm{N}-1) + \chi^2 \times \mathrm{p} \times (1-\mathrm{p})}$$

where, χ^2 (=3.84) is the table value of chi-square for 1 degree of freedom and 95% of confidence level, p (=0.5) is the population proportion and e (=0.05) is the degree of accuracy. N and n, representing the population size and the required sample size, were 305,004 and 1,469, respectively, based on ionogram data collected exclusively during winter seasons over a five-year period. The population proportion (p) of 0.5 was used to provide the maximum sample size. The sample data were randomly chosen for specific season and local time and evaluated by manually comparing the produced density profiles with corresponding ionogram images. Table 2 shows the misclassification ratio for each season from the observation period of 2017 to 2021. This table indicates that the misclassification ratio was less than 3% and slightly higher only in the austral winter (i.e., during polar night), which may indicate that the polar ionosphere tends to be more disturbed in winter.

The variation of misclassification ratio with time is presented in Fig. 4. The local time at JBS is UT + 11 hr and the magnetic local time is shifted further by 4.7 hr calculated by Altitude-Adjusted Corrected GeoMagnetic (AACGM) at the location of JBS. The magnetic local midnight and noon are marked with solid and open circles, respectively at the top of the Fig. 4. The misclassification ratio is estimated to be from about 1.5% to 3.0%, peaking at around 15 UT (i.e., 02LT or 07MLT). The ratio is largely greater in the magnetic morning sector than the magnetic evening to midnight sector. Assuming that the ionospheric density profiles are severely disturbed during auroral occurrence, the enhanced misclassification ratio in the morning sector seems to associated with the large auroral occurrence over the JBS in

Table 2. Results of the ratio of misclassification for each season during the period from 2017 to 2021

Season	Spring	Summer	Autumn	Winter
Misclassification ratio (%)	1.67	1.84	1.70	2.31

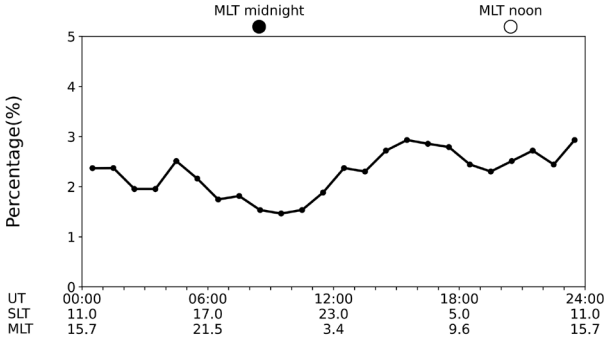


Fig. 4. Temporal variations of the misclassification ratio with universal time (UT), solar local time (SLT), and magnetic local time (MLT). The magnetic midnight and noon are marked at the top of the panel.

the morning sector (Jee et al. 2021).

Fig. 5 shows the classification results in the form of temporal variations for four types of ionograms presented in Fig. 3 during the entire observation period of 2017–2021: Black, red, blue, and green colors denote 'Unavailable', 'Sporadic E', 'Needs Reprocessing', and 'Available' types, respectively. The solid and open circles at the top of the panel indicate magnetic local midnight and noon. The occurrence ratio shows noticeable dependencies on the magnetic local time. The 'Unavailable' types tend to be more frequent near the magnetic morning sector. This result may be related to the largest auroral occurrence observed by auroral all sky camera (ASC) at JBS (Jee et al. 2021). In other words, auroral particles may disturb the ionospheric density, thereby affecting the ionospheric sounding radar observations in the region.

The occurrence of 'Sporadic E' was fairly large up to almost 50% at the early evening and decreased to a minimum (about 20%) at around the magnetic midnight: the average occurrence was about 35%–40%. This result indicates that the sporadic-E like structures in the lower atmosphere are the main obstacles to observing the F-region ionosphere in the sounding observations of the polar ionosphere. It is well known that the auroral precipitations in the polar region are one of the main sources of enhanced ionization in the E-region ionosphere (Kirkwood & Nilsson 2000). The occurrence ratio of 'Sporadic E' presented in Fig. 5 may provide an important information for the study on the sporadic E in the polar region in association with the characteristics of the location of JBS. The 'Needs Reprocessing' type also tends to increase in the magnetic morning sector, suggesting a relation to the auroral disturbances strong enough to prevent SNR measurement,

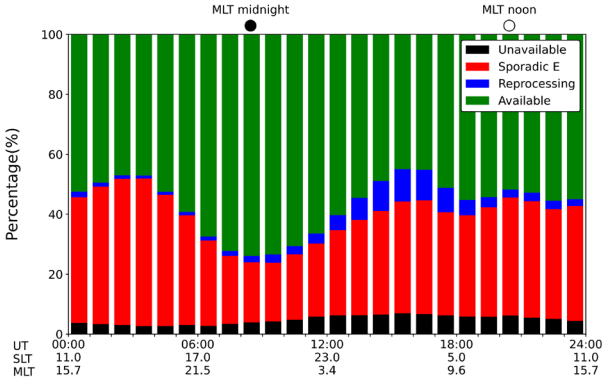


Fig. 5. Temporal variations of the percentage ratio of four types (different colors) based on the data during the entire observation period from 2017 to 2021 with universal time (UT), solar local time (SLT), and magnetic local time (MLT). The magnetic midnight and noon are denoted at the top of the panel.

similar to those associated with the 'Unavailable' type. Finally, the occurrence of 'Available' type is maximized near the magnetic local midnight but decreases in the dayside, which seems to be closely associated with the occurrences of 'Sporadic E'. However, identifying the dominant mechanisms of sporadic E formation at high latitudes lies beyond the scope of this study and is left for future work.

5. SUMMARY AND CONCLUSION

We developed an automatic classification procedure for the ionograms obtained from VIPIR/Dynasonde ionospheric radar at JBS, Antarctica in order to flag ionospheric data products from the autonomous Dynasonde analysis that require special treatment, for example, the Expert Reprocessing feature of the Dynasonde web interface (http://surf.colorado.edu/login.dcc). This procedure classifies the ionograms into four types with only about 2% of misclassification. It was found that approximately 55% of the data is available for the specification of the F-region ionosphere without any alterations, about 35% of the data shows sporadic-E like structures which are blocking out the radio signal from proceeding into the F-region ionosphere, about 5% is unavailable for extraction of the ionospheric parameters, and about 5% require initiation of the re-analysis procedure using Expert Reprocessing feature. With regard to the local time variations of each type, the available data are closely related to the sporadic-E like structure and unavailable and reprocessing types seem to be associated with auroral precipitations over JBS.

ACKNOWLEDGMENTS

This work was supported by Korea Polar Research Institute (KOPRI) grant funded by the Ministry of Oceans and Fisheries (KOPRI PE25020).

ORCIDs

Junho Back https://orcid.org/0009-0000-8457-3049
Geonhwa Jee https://orcid.org/0000-0001-7996-0482
Hyuck-Jin Kwon https://orcid.org/0000-0001-9670-0711
Khan-Hyuk Kim https://orcid.org/0000-0001-8872-6065
Changsup Lee https://orcid.org/0000-0003-4046-7089
Young-Bae Ham https://orcid.org/0000-0002-1714-0638
Nikolay Zabotin https://orcid.org/0000-0003-0715-1082

REFERENCES

Afolayan AO, Jit Singh M, Abdullah M, Buhari SM, Yokoyama T, et al., Observation of seasonal asymmetry in the range spread F occurrence at different longitudes during low and moderate solar activity, Ann. Geophys. 37, 733-745 (2019). https://doi.org/10.5194/angeo-37-733-2019

Carlson HC Jr, The dark polar ionosphere: progress and future challenges, Radio Sci. 29, 157-165 (1994). https://doi.org/10.1029/93RS02125

Fontaine D, Structure and dynamics of the Earth's polar ionosphere: recent results inferred from incoherent scatter sounders, Plasma Sources Sci. Technol. 11, A113 (2002). https://doi.org/10.1088/0963-0252/11/3A/317

Ham YB, Jee G, Lee C, Kwon HJ, Kim JH, et al., Observations of the polar ionosphere by the vertical incidence pulsed ionospheric radar at Jang Bogo Station, Antarctica, J. Astron. Space Sci. 37, 143-156 (2020). https://doi.org/10.5140/JASS.2020.37.2.143

Heelis RA, The polar ionosphere, Rev. Geophys. 20, 567-576 (1982). https://doi.org/10.1029/RG020i003p00567

Jee G, Ham YB, Choi Y, Kim E, Lee C, et al., Observations of the Aurora by visible all-sky camera at Jang Bogo Station, Antarctica, J. Astron. Space Sci. 38, 203-215 (2021). https://doi.org/10.5140/JASS.2021.38.4.203

Kim E, Jee G, Ham YB, Zabotin N, Lee C, et al., Assessment of polar ionospheric observations by VIPIR/Dynasonde at Jang Bogo Station, Antarctica: part 1—ionospheric densities, Remote Sens. 14, 2785 (2022). https://doi.org/10.3390/rs14122785

Kim KH, Kim DH, Back J, Kwon HJ, Jee G, et al., Dynasonde observations of ionospheric polar holes under quiet geomagnetic conditions at Jang Bogo Station, Antarctica, J. Geophys. Res. Space Phys. 128, e2023JA031563 (2023). https://doi.org/10.1029/2023JA031563

Kintner PM, Ledvina BM, de Paula ER, GPS and ionospheric scintillations, Space Weather. 5, S09003 (2007). https://doi.org/10.1029/2006SW000260

Kirkwood S, Nilsson H, High-latitude sporadic-E and other thin layers – the role of magnetospheric electric fields, Space Sci. Rev. 91, 579-613 (2000). https://doi.org/10.1023/A:1005241931650

Krejcie RV, Morgan DW, Determining sample size for research activities, Educ. Psychol. Meas. 30, 607-610 (1970). https://doi.org/10.1177/001316447003000308

Kwon HJ, Jee G, Ham YB, Zabotin N, Lee C, et al. Assessment of polar ionospheric observations by VIPIR/Dynasonde at Jang Bogo Station, Antarctica: 2. Ionospheric ion drift velocity, J. Geophys. Res. Space Phys. 129, e2023JA032402 (2024). https://doi.org/10.1029/2023JA032402

Kwon HJ, Kim KH, Jee G, Seon J, Lee C, et al., Disappearance of the polar cap ionosphere during geomagnetic storm on 11 May 2019, Space Weather. 20, e2022SW003054 (2022). https://doi.org/10.1029/2022SW003054

Kwon HJ, Lee C, Jee G, Ham YB, Kim JH, et al., Ground-based observations of the polar region space environment at the Jang Bogo Station, Antarctica, J. Astron. Space Sci. 35, 185-193 (2018). https://doi.org/10.5140/JASS.2018.35.3.185

Piggott WR, Rawer K, URSI handbook of ionogram interpretation and reduction, Technical Report, Report UAG ; 23A (1978).

Scali JL, Reinisch BW, Kelley MC, Miller CA, Swartz WE, et al., Incoherent scatter radar and Digisonde observations at tropical latitudes, including conjugate point studies, J. Geophys. Res. 102, 7357-7367 (1997). https://doi.org/10.1029/96JA03519

Shepherd SG, Altitude-adjusted corrected geomagnetic coordinates: definition and functional approximations, J. Geophys. Res. Space Phys. 119, 7501-7521 (2014). https://doi.org/10.1002/2014JA020264

Wang N, Guo L, Ding Z, Zhao Z, Xu Z, et al., Longitudinal differences in the statistical characteristics of ionospheric spread-F occurrences at midlatitude in Eastern Asia, Earth Planets Space 71, 47 (2019). https://doi.org/10.1186/s40623-019-1026-6

Wright JW, Pitteway MLV, A new data acquisition concept for digital ionosondes: phase-based echo recognition and real-time parameter estimation, Radio Sci. 34, 871-882 (1999). https://doi.org/10.1029/1999RS900039

Zabotin NA, Wright JW, Zhbankov GA, NeXtYZ: three-dimensional electron density inversion for dynasonde ionograms, Radio Sci. 41, RS6S32 (2006). https://doi.org/10.1029/2005RS003352